Journal of Quantitative Spectroscopy & Radiative Transfer 228 (2019) 1–10

Contents lists available at ScienceDirect

Journal of Quantitative Spectroscopy & Radiative Transfer

journal homepage: www.elsevier.com/locate/jqsrt

Enhanced backscatter of vortex beams in double-pass optical links with atmospheric turbulence

Jiayi Yu[a,b], Yan Huang[a], Greg Gbur[b], Fei Wang[a,*], Yangjian Cai[a,c,*]

[a] School of Physical Science and Technology & Collaborative Innovation Center of Suzhou Nano Science and Technology, Soochow University, Suzhou 215006, China

[b] Department of Physics and Optical Science, University of North Carolina at Charlotte, Charlotte, NC 28223, USA

[c] Shandong Provincial Engineering and Technical Center of Light Manipulations & Shandong Provincial Key Laboratory of Optics and Photonic Device, School of Physics and Electronics, Shandong Normal University, Jinan 250014, China

ARTICLE INFO

Article history:
Received 22 December 2018
Revised 2 February 2019
Accepted 17 February 2019
Available online 18 February 2019

Keywords:
Enhanced backscatter
Vortex beam
Atmospheric turbulence
Propagation

ABSTRACT

Though the enhanced backscatter (EBS) of waves passing through monostatic turbulence has been explored extensively over the past few decades, studies have been confined to spherical, planar, or Gaussian waves. Here we experimentally investigate the EBS of Laguerre–Gaussian (LG) vortex beams on double passage through turbulent air, reflecting from a retroreflector. It is found that only vortex beams with an even topological charge exhibit EBS, whereas beams with an odd topological charge maintain a dark-hollow shape. It is also found from observing instantaneous beam profiles that vortex modes can convert from LG to Hermite–Gaussian (HG) form. The physical mechanisms behind the aforementioned effects are explained using a ray model, and the results are further confirmed computationally using a multiple phase screen method. This work potentially allows the control of EBS through engineering the phase in the transmitter plane.

1. Introduction

When a light wave makes a double pass through a random medium which is effectively unchanging over the propagation time, i.e. monostatic turbulence, it experiences an increase of mean irradiance close to the optical axis, referred to as enhanced backscatter (EBS). This phenomenon was first predicted by Belen'kii and Mironov [1], and later was experimentally observed in both the lab and in the atmosphere [2,3]. Owing to its importance in laser radar systems, EBS and related double-passage problems have been extensively studied both in theory [4–7] and in experiment [8,9]. The EBS effect has found potential use in precision pointing and tracking [10,11] as well as imaging [12]. Recently, double-passage problems have found renewed interest with the development of modulating retroreflector (MRR) technology in free-space optical communications (FSOC) [13–18]. In such systems, an MRR combines an optical retroreflector with a modulator to reflect a modulated signal directly back to a receiver. An understanding of EBS is therefore important in MRR systems. The enhancement of scintillation of a reflected beam through outdoor turbulence was investigated in [16]. The features of EBS created via a retroreflector in lab-generated classical and non-classical turbulence were investigated in [19,20].

In these earlier studies, the optical waves considered were limited to spherical waves, plane waves, and Gaussian beams. In recent years, however, considerable attention has been paid to vortex beams [21–33] due to their potential applications in FSOC communications and optical images. Such beams possess an intensity minimum on axis and a helical phase structure in the form of $\exp(il\varphi)$, where l is the topological charge and φ is the azimuthal angle. As one knows, light beams will experience beam wander, scintillation and angle-of-arrival fluctuation when they propagate in atmospheric turbulence. However, some studies showed that vortex beams can greatly reduce these negative effects [21–23]. In addition, as vortex beams with different topological charges are mutually orthogonal, they have been applied to increase the data rate in FSOC by multiplexing information on different vortex modes simultaneously [24]. Mode mixing [25,26] and degradation of mode quality resulting in cross-talk between orbital angular momentum (OAM) modes [27,28] were investigated when the phases of vortex beams suffered random fluctuation induced by turbulence. The possible use of vortex beams for communications in photon count-

* Corresponding authors.
E-mail addresses: fwang@suda.edu.cn (F. Wang), yangjiancai@suda.edu.cn (Y. Cai).

https://doi.org/10.1016/j.jqsrt.2019.02.021

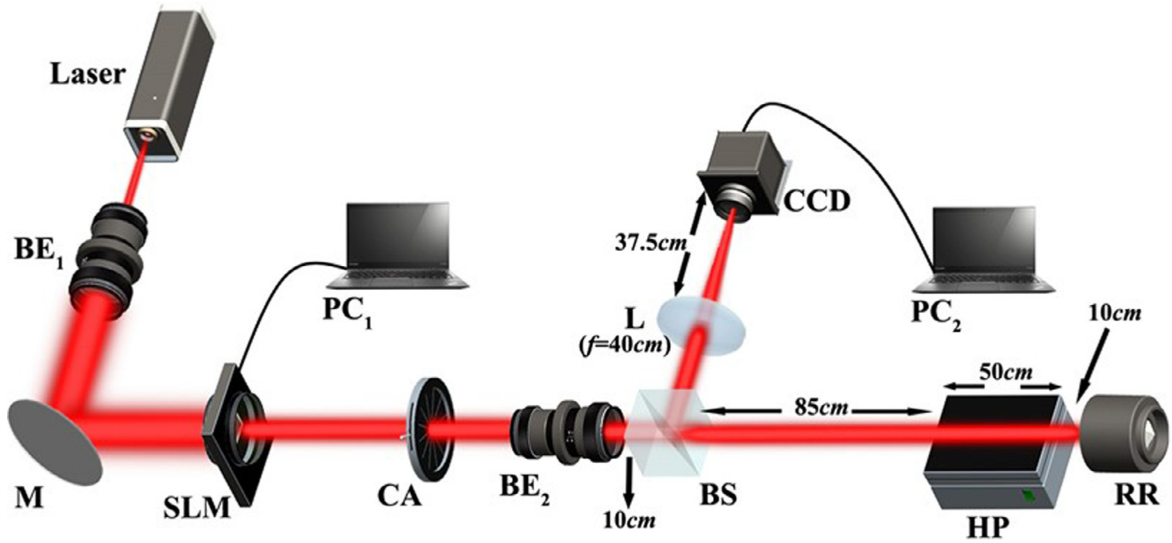

Fig. 1. Schematic of the experimental setup for the generation of vortex beams and measurement of the intensity distributions through a monostatic double-passage channel.

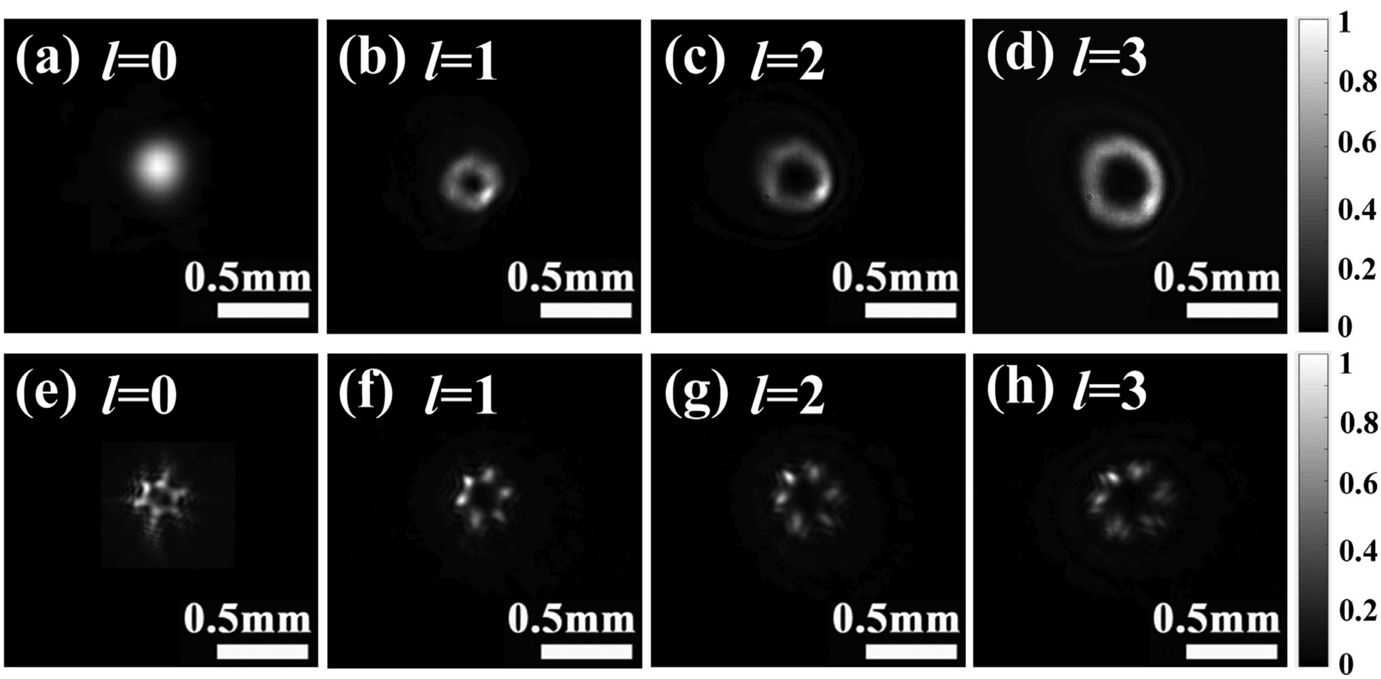

Fig. 2. Density plot of the beam profiles of the Gaussian beam ($l = 0$) and vortex beams ($l = 1$, 2, 3) in the receiver plane reflected by a flat mirror (first row) and retroreflector (second row).

ing level was studied in [29,30]. Recently, Yuan et al. proposed an optimized scheme to improve the detection probability of OAM of vortex both in Kolmogorov and non-Kolmogorov turbulence [31].

In this paper, we explore both the average and instantaneous behavior of vortex beams on double-passage through monostatic turbulence via a retroreflector. We find that EBS only appears for beams with even topological charge, while beams with odd charge maintain their intensity minimum. It is further found that Laguerre–Gauss (LG) vortex modes will convert to Hermite–Gauss (HG) modes under certain circumstances. Physical explanations of these effects are presented.

2. Experimental results and analysis

The experimental arrangement is illustrated in Fig. 1. A linearly polarized Gaussian beam generated from a He-Ne laser ($\lambda = 632.8\,\mathrm{nm}$) is first passed through a beam expander (BE_1) and then reaches a spatial light modulator (SLM) acting as a computer-controlled (PC_1) phase screen. A standard fork grating [34] is programmed onto the SLM to generate the desired vortex beam of azimuthal order l; a circular aperture (CA) is used to isolate only the desired vortex diffraction order from the SLM. The resulting vortex beam is then expanded and collimated by BE_2.

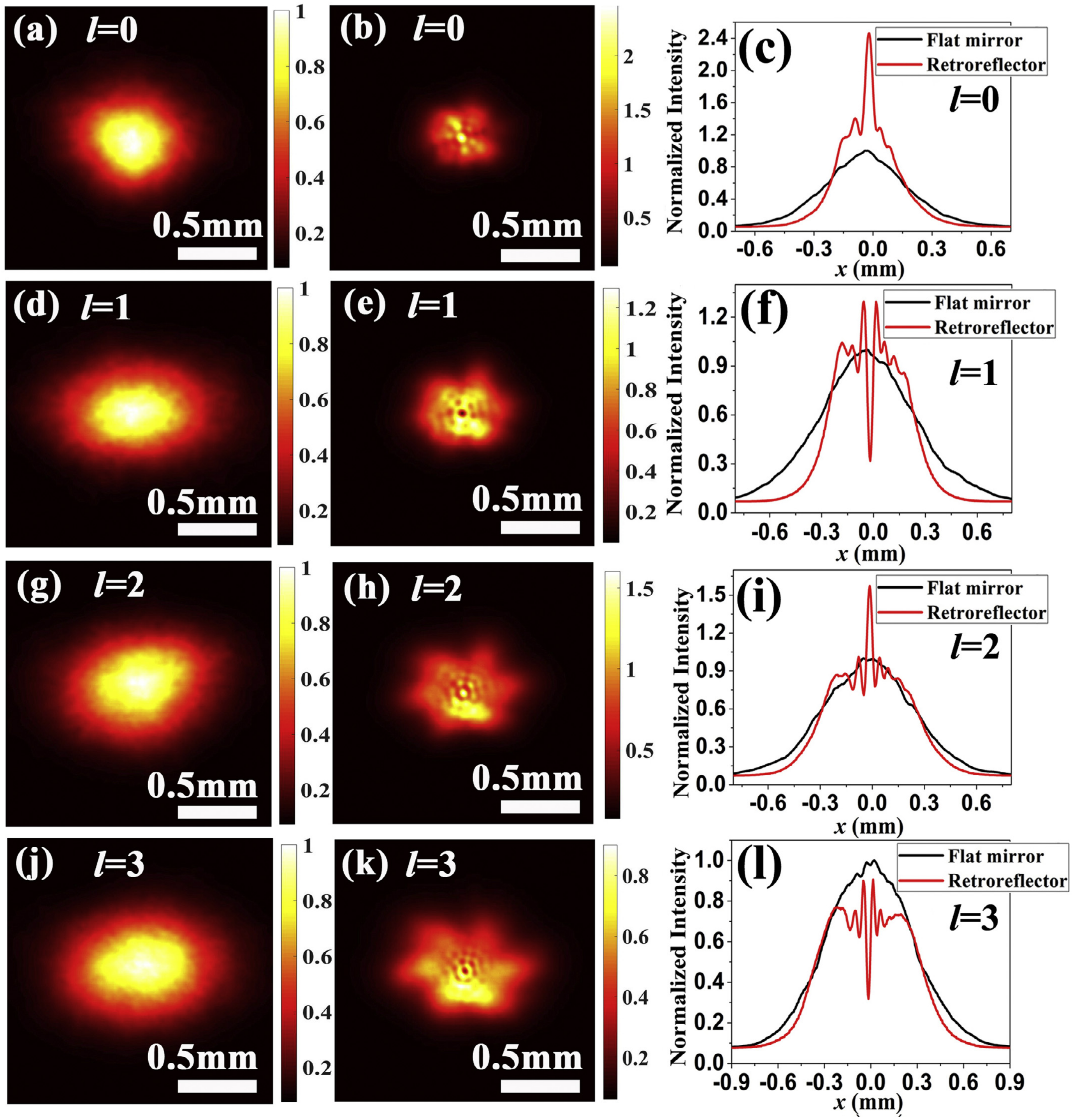

Fig. 3. Density plot of the beam profiles of the Gaussian beam ($l = 0$) and vortex beams for different values of topological charges reflected by a flat mirror (first column) and retroreflector (second column). The corresponding cross-line of the intensity distribution at $y = 0$ is plotted in the third column.

After the expander BE_2, the beam is well-represented as an LG mode with radial index 0 and azimuthal index l [24]

$$E(r, \varphi, z = 0) = A_l r^l \exp\left(-\frac{r^2}{\omega_0^2}\right) \exp(il\varphi), \tag{1}$$

where $r=(x^2+y^2)^{1/2}$ and φ are the radial and azimuthal coordinates, respectively. A_l is a positive constant; l is the topological charge. When $l = 0$, this expression reduces to a fundamental Gaussian mode. The measured beam width ω_0 after BE_2 is almost the same for $l = 1, 2, 3$, with $\omega_0 = 2.5$ mm.

A beam splitter (BS) sends half of the resulting intensity through atmospheric turbulence generated by a hot plate (HP), after which it reflects off a retroreflector (RR), and then returns back via the same path. The type of the RR used is the corner reflector, a commercial product of Thorlabs. Such reflector is a set of three mutually perpendicular reflective surfaces manufactured

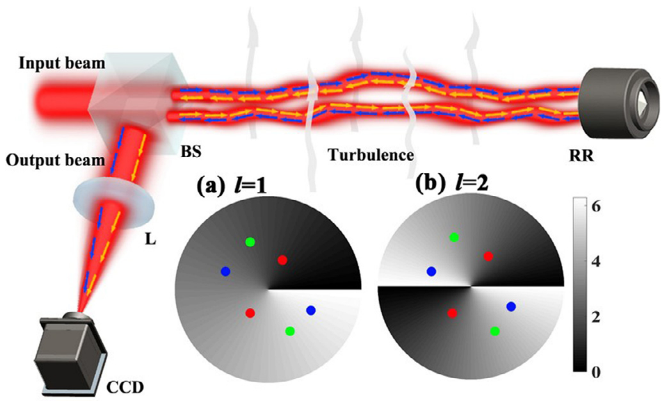

Fig. 4. Diagram of a reciprocal ray pair (denoted by blue and yellow arrows) of the input beam propagation through the turbulence reflecting from retroreflector. Inset figures (a) and (b) are the phase map of vortex beams for $l=1$ and 2, respectively. The initial phase difference of the red, green or blue two-point pairs in vortex beams with $l=1$ and 2 are π (out of phase) and 2π (in phase), respectively.

from a solid piece of N-BK7 glass, which form the corner of a cube. It reflects a beam back toward its original direction via three total internal reflections, but the reflected beam rotates 180° with respect to the incident beam. The backward beam is reflected by the BS and is focused by a lens (L) with focal length 40 cm. A CCD with 1952×786 square pixels of side length 3.75 µm is placed at the receiver plane to measure the average/instantaneous intensity distributions, the distance between the CCD and the lens is 37.5 cm. The integrated time of the CCD is set to be 50µs. The measured intensity was averaged over 2000 frames with frame per second (FPS) of the CCD being 25.

2.1. Enhanced backscatter

Before performing the experiment in the turbulence, we first investigate the beam profiles of LG beams in the receiver plane free of turbulence. Fig. 2(a)–(d) show the intensity distributions of LG beams with different topological charges reflected by a flat mirror. In this case, a flat mirror is used in placed of the RR and the hot plate is turned off. Fig. 2(e)–(h) illustrate the corresponding beam profiles reflected by the RR in the receiver plane. As shown in Fig. 2(a)–(d), the beam patterns of LG beams with $l=1$, 2, 3 keep dark hollow shapes, indicating that the phase singularity at the central point still exists. In the case of the RR, the beam patterns for $l=0$, 1, 2, 3 are all divided into six beamlets, while the intensity at the central point is zero. This phenomenon can be explained by the fact that the RR used in the experiment is not an ideal RR. There is a linear defect at the junction of two reflective surfaces. Therefore, totally three linear defects exist in the RR, which divide the incident beam into six beamlets after reflection. Owing to these defects, the unexpected “scatter light” from the defects will be focused in the focal plane of the lens, which interferes with the EBS effect. To avoid to the “scatter light”, we place the CCD after the lens 37.5 mm, not the focal plane $f=40$ mm.

Now, we turn to examine the average intensity of vortex beams passing through the double-passage channel in presence of turbulence. The temperature of the hot plate is set to be 160 °C. For comparison, both a flat mirror and a retroreflector were used to produce the reflected beam. Fig. 3 illustrates the experimental average intensity profiles of a Gaussian beam ($l=0$) and vortex beams with $l=1$, 2, 3 reflected by the flat mirror (first column) and the retroreflector (second column), respectively. The corresponding cross-sections of the intensities at $y=0$ are plotted in the third column in Fig. 3. For each example, the average intensity pattern is normalized by the intensity maximum reflected by the flat mirror. Note that the size of the mirror and retroreflector is much larger than that of the beam spot. the reflectors can thus be considered as infinite. One can see that the beam profiles of vortex beams degenerate to Gaussian-like shapes for the case of the flat mirror, irrespective of topological charge. When the retroreflector is used, the situation is different. The average intensity for $l=0$, 2 exhibits a sharp and bright peak in the beam center, indicative of an EBS enhancement. The central peak values for $l=0$ and 2 are about 2.46 and 1.60 compared to these for flat mirror target. According to Chapter 2 of Ref. [4], the calculated amplification factor used our experimental parameters is about 1.9, lower than that in our experiment. There are some factors that cause the deviation between the experimental and theoretical results, such as turbulence models, beam models and especially for the RR used in the experiment, which is not ideal. For $l=1$ and $l=3$, however, the beam profiles still display dark-hollow shapes, with no EBS. Other experimental results for higher values of l (not shown here) indicate that EBS only occurs when the topological charge is an even number.

The experimental results suggest that the EBS is strongly dependent on the phase distribution of the incident beam. To qualitatively explain the results, we consider a ray model of propagation through the system. A collimated beam consists of many individual rays with zero transverse wavenumber starting from the transmitter plane. These rays follow a deviated path due to the random index fluctuations of the medium, and EBS results when many pairs of these rays, referred to as reciprocal pairs, follow identical but opposite double paths through the turbulence, as illustrated in Fig. 4 for a blue-yellow pair. Because this reciprocal pair has traveled an identical optical path length through the medium, it arrives at the detector with a definite phase relation; pairs following different paths will generally have a random phase relation. As is known, a retroreflector inverts the wavefront in the x and y-axis simultaneously, equivalent to a 180° rotation of the back-propagating beam. This indicates that rays which lie in symmetric positions on opposite sides of the beam axis are most likely to form reciprocal pairs [see the red, green or blue two-point pairs in Fig. 4(a) and (b)]. For a uniform beam such as a Gaussian or plane wave, the reciprocal pairs will arrive in phase, resulting in EBS. For vortex beams, an even-charge vortex will have reciprocal wave pairs that are in phase, as in Fig. 4(b), but an odd-charge vortex will have reciprocal wave pairs that are out of phase, as in Fig. 4(a). This ray model therefore predicts, in agreement with experiment, that odd-charge vortex beams will have destructive interference in their center, and a dark core, while even-charge vortex beams will have constructive EBS.

For an ordinary mirror, fewer reciprocal pairs exist relative to a retroreflector, resulting in less EBS. In addition, the turbulence-induced tilt aberration cannot be compensated by the flat mirror. Thus, the beam spot will drift randomly in the receiver plane which is induced by the random fluctuations of the index-of-refraction of the atmosphere, known as wandering effect. As a consequence, this effect will wash out any remaining EBS in the receiver plane, and lead to the degradation of the beam profile into a Gaussian-like shape in the receiver plane.

2.2. Mode conversion

Let us now investigate the instantaneous behavior of vortex beams in the receiver plane. Surprisingly, we find from experiment that the beam mode will often convert from the LG_{0l} mode to its corresponding HG_{l0} mode, but with the x-axis oriented randomly. Fig. 5 illustrates the instantaneous intensity distributions in the re-

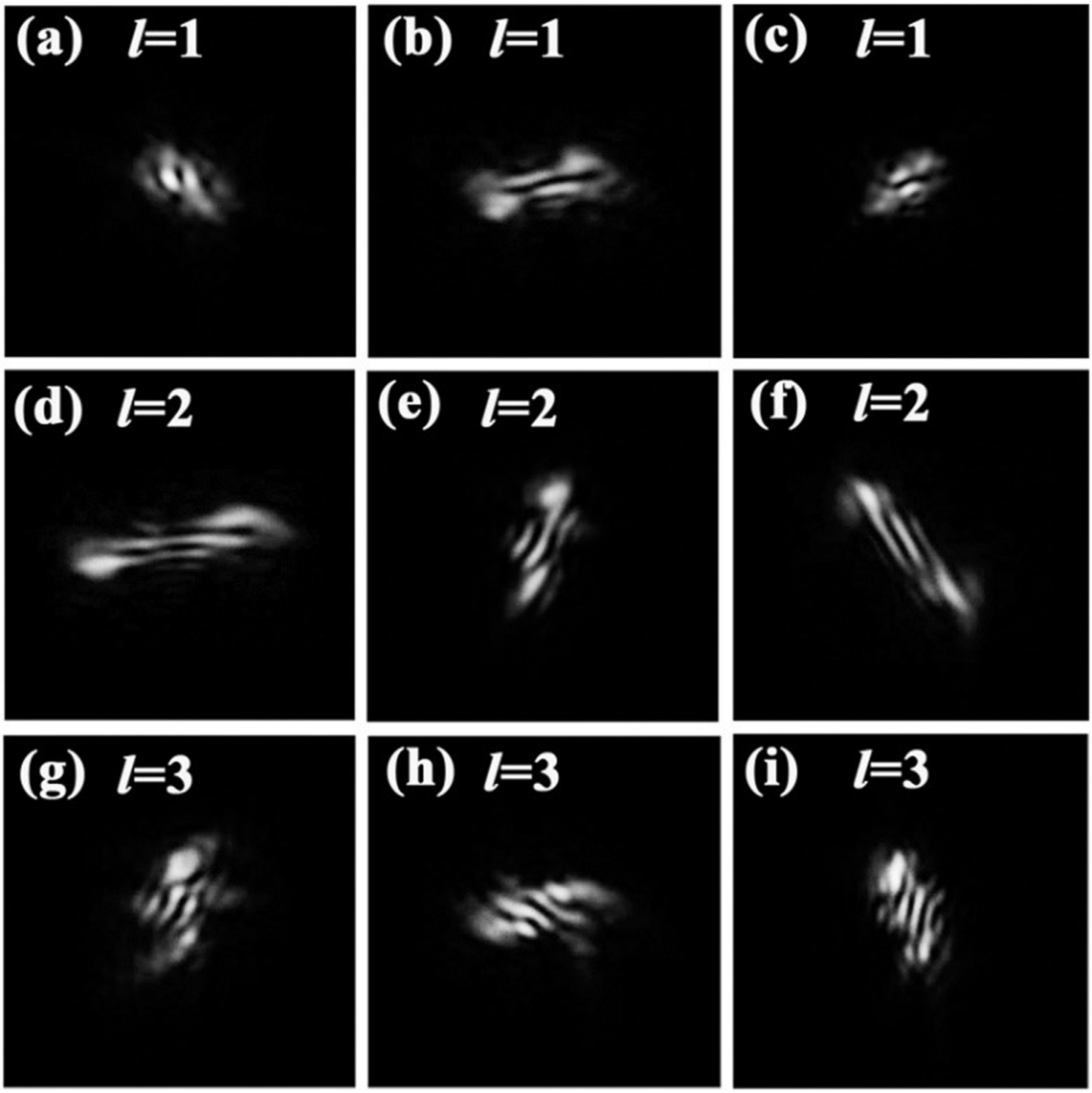

Fig. 5. Experimental results of instantaneous beam profiles of vortex beams for different values of topological charges in the receiver plane reflecting from retroreflector. (a)–(c) $l = 1$ [media 1]; (d)–(f) $l = 2$ [media 2]; (g)–(i) $l = 3$ [media 3]. The size of pictures is 1.5 mm × 1.5 mm.

ceiver plane after reflecting from the retroreflector. One finds that the beam mode becomes a quasi HG_{l0} mode, with the characteristic l intensity nulls along the axis of symmetry. The probability of mode conversion is about 35.08% for $l = 1$ from 1000 pictures captured by the CCD, and decreases to 27.47% and 20.92% for $l = 2$ and $l = 3$, respectively. To explain this mode conversion, we can adapt the aforementioned explanation for the EBS phenomenon. When l is even, the HG_{l0} mode possesses a bright spot in the beam center [see in Fig. 5(d)–(f)], while it is dark for l being odd [see in Fig. 5(a)–(c) and Fig. 5(g)–(i)]. If we average over the intensity distribution for enough realizations, it is expected that only the beam profiles of even-order vortex beams contribute to the bright spot in the center, implying EBS enhancement. We should emphasis that the mode conversion effects are also observed in flat mirror case, but the position of the beam randomly wanders, eliminating EBS on average.

The occurrence of the observed mode conversion is closely related to the strength of turbulence (temperature of the hot plate). When the strength of the turbulence is above or below an optimal value, the probability of mode conversion gradually decreases. It is known that the instantaneous beam profiles in the receiver plane are closely related to the inner scale and the strength of turbulence. If the size of the inner scale is much smaller than the beam width and transverse coherence width, the beam splits into several pieces on propagation and develops into speckles, while a larger inner scale leads to a beam with lens-like refractive phase

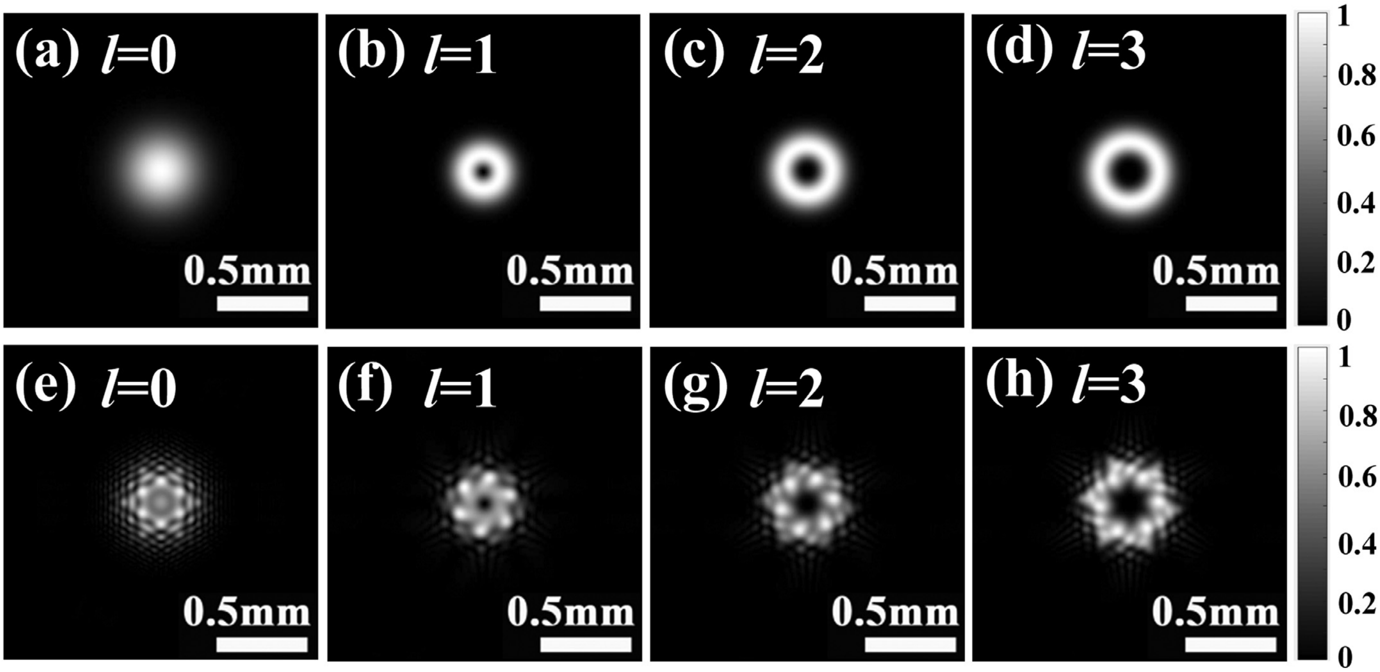

Fig. 6. Simulation results of beam profiles of the Gaussian beam ($l=0$) and vortex beams ($l=1$, 2, 3) in the receiver plane without turbulence. (a)–(d) reflected by a flat mirror, (b)–(d) reflected by a RR.

variations in the turbulence. In our experiment, the estimated inner scale generated by the hot plate is about in the range 2 mm–6 mm, comparable to the beam width. The instantaneous lens-like refractive variations may occasionally be anisotropic, like the phase induced by the cylindrical lens [35]. Since cylindrical lenses can induce mode conversion, under such circumstances the turbulence plays the same role.

This mode conversion is likely associated with the exchange of the orbital angular momentum (OAM) between the vortex beam and the turbulent medium. Although Ref. [24] declared that the OAM is conserved when vortex beams propagate through atmospheric turbulence, this result applies to the statistical average. Therefore, we may conclude that, instantaneously, the OAM can couple from the beam to the turbulent media or from the turbulent media to the beam but, averaging over a long time, the OAM of the beam remains unchanged.

3. Simulation results

Some analytical approaches have been developed to deal with the propagation of light beam through a double-pass link with atmospheric turbulence based on Rytov approximation [Chapter 13 in Ref. [36]], but these approaches are rather complicated and only applicable for the plane waves, spherical waves and Gaussian waves. Besides analytical approaches, a numerical method, named a multi-phase screen method, is widely applied for simulating the propagation of light waves in atmospheric turbulence numerically. In this method, the extended random media is modeled as a collection of thin random phase screens with appropriated statistics of turbulence. In principle, it can deal with the propagation of various types of laser models through turbulence with different statistics. Therefore, in this section, we perform simulations with the multi-phase screen method to support our experimental results.

The detailed description of the algorithm can be found in [37–40]. In the simulation, the size of the phase screen is 40 mm × 40 mm with a 512 × 512 grid. The single path length L is 1.5 m. The power spectral density of the turbulence is chosen as the Von Kaman spectrum [36], given by

$$\Phi_n(\kappa) = 0.033C_n^2\left(\kappa^2+\kappa_0^2\right)^{-11/6}\exp\left(-\kappa^2/\kappa_m^2\right), \tag{2}$$

where $\kappa = (\kappa_x^2+\kappa_y^2)^{1/2}$ is the transverse spatial frequency, C_n^2 is the structure constant of the turbulence. $\kappa_m = 5.92/l_0$ with l_0 being the inner scale of turbulence, and $\kappa_0 = 2\pi/L_0$ with L_0 being the outer scale of turbulence.

A double-passage link in the turbulence uses six phase screens: three for from the transmitter plane to the reflector and three for the backward path. The three phase screens are equally divided into the forward/backward paths. As the turbulence is monostatic, the same phase screens are used for both paths. If the target is a retroreflector, the optical field in the target plane flips along x-axis and y-axis simultaneously, while the above flip operation is absent when the target is a flat mirror. At the end of the backward path, the field is focused by the lens with focal length 40 cm. A two-step propagation algorithm is used to calculate the optical fields from the lens to the receiver plane [37]. The distance between the lens and receiver plane is 37.5 cm. The average intensity is obtained using 1000 runs through statistical independent phase screens.

In the following numerical simulation, the parameters are chosen to be $l_0 = 4$ mm, $L_0 = 0.5$ m, $\lambda = 632.8$ nm, $\omega_0 = 2.5$ mm. Fig. 6 presents the intensity distributions of the Gaussian beam and the vortex beams in the receiver plane reflected by a flat mirror [Fig. 6(a)–(d)] and a RR [Fig. 6(e)–(h)]. The turbulence is absent ($C_n^2 = 0$) in this simulation. In order to mimic three linear defects of the real RR in the experiment, we introduce three single slits placed in the RR plane in the numerical simulation. The three single slits equally separate the RR plane six parts and two adjacent slits form an angle 60°. The widths of the silts are all chosen to be 0.4 mm and the transmission coefficient is zero. In the case of the flat mirror, the above operation is cancelled. It can be seen from Fig. 6(a)–(d) that the beam shape of the Gaussian beam and

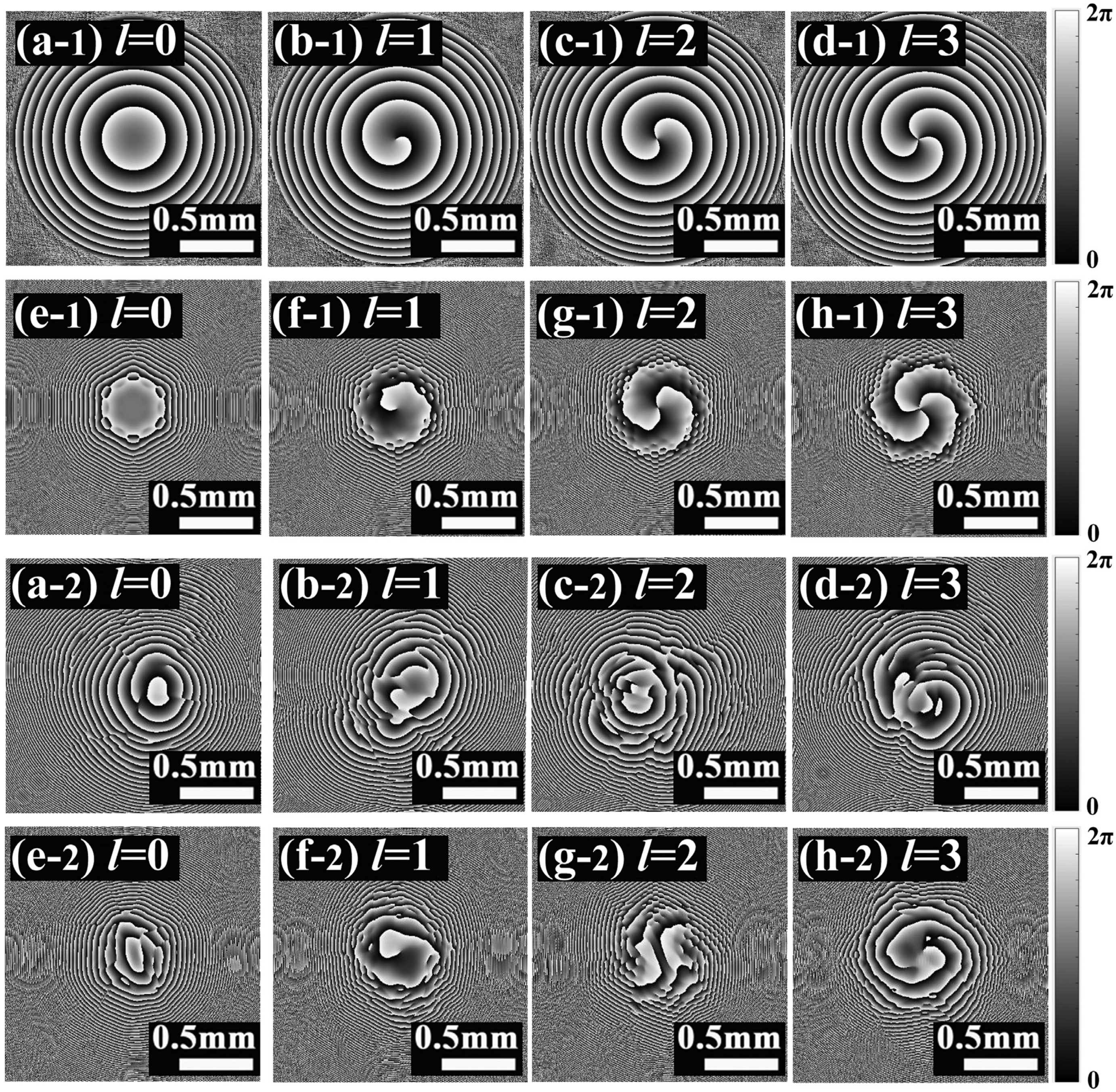

Fig. 7. Simulation results of phase patterns of the Gaussian beam and vortex beams in the receiver plane with [(a-2)-(h-2)] and without [(a-1)–(h-1)] turbulence. (a-1)–(d-1) and (a-2)–(d-2): reflected by a flat mirror; (e-1)– (h-1) and (e-2)–(h-2): reflected by a RR.

the vortex beam keep invariant after reflected from the flat mirror, only the size of beam spot is reduced in the receiver plane, as expected. The beam profiles reflected by the RR are divided into six parts and the singularity at the on-axis point can still be observed for $l = 1$, 2, 3, while the intensity at the central point for $l = 0$ is not zero. Compared the simulation results with those in Fig. 2, it is found that the simulation results and experiment results in the case of RR are slightly different. The reason is that the use of three slits to mimic the linear defects in real RR is not a perfect way. However, the behaviors of the average intensity passing through turbulence between the simulation results and experimental results are almost the same, which we will describe later. Note that if the three slits are removed in the simulation, i.e., the perfect RR, the intensity distributions between the flat mirror and the RR are exactly the same.

In Fig. 7, we present the instantaneous phase profiles of the Gaussian beam and the vortex beams with (C_n^2=1.5 × 10$^{-9}m^{-2/3}$) and without (C_n^2= 0) turbulence in the receiver plane. In the absence of turbulence, the phase distribution of the Gaussian beam ($l = 0$) become a spherical phase due to that the quadratic phase factor is introduced by free-space propagation and a thin lens. The phase distributions of the vortex beams ($l = 1$, 2, 3) become the

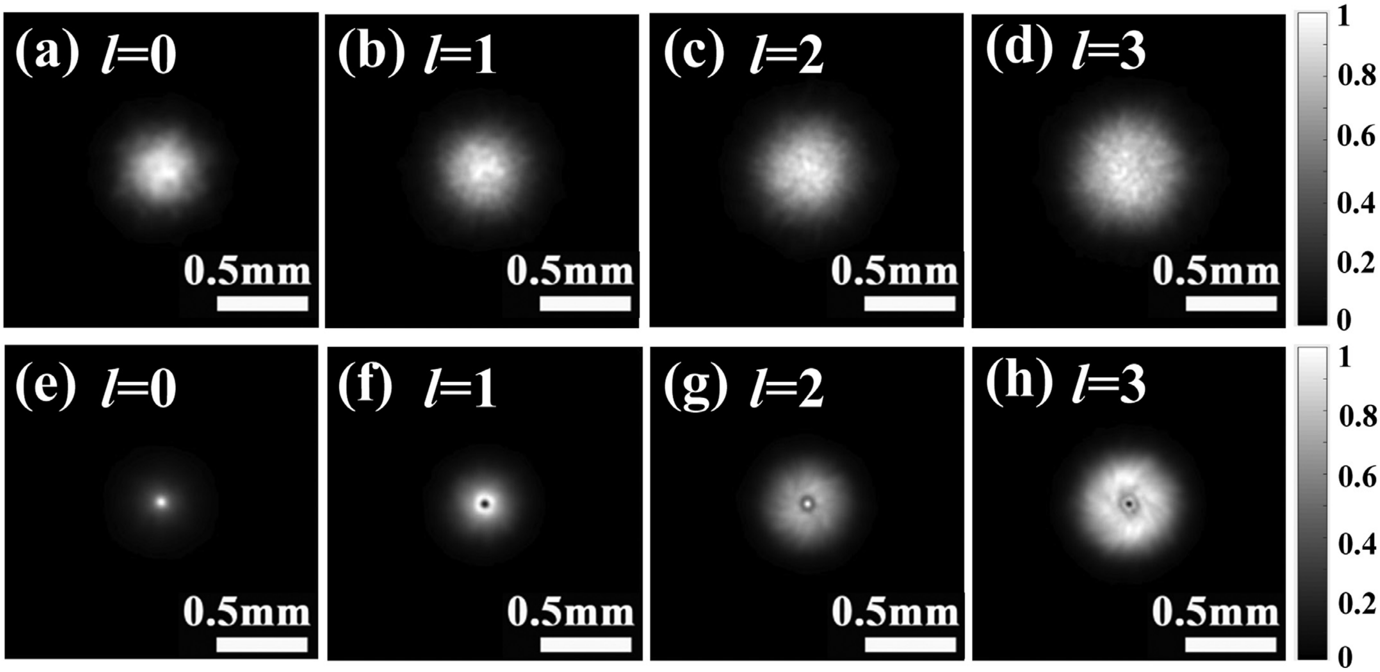

Fig. 8. Simulations results of the average beam profiles of the Gaussian beam and vortex beams in the receiver plane. The structure constant is C_n^2=1.5 × $10^{-9}m^{-2/3}$. The size of pictures is 1.5 mm × 1.5 mm.

multiplication of the spherical phase factor and the spiral phase factor. In the case of the RR, the phase distributions near the central region (|r| < 0.5 mm) are similar to those reflected by a flat mirror, expect for the 180° rotation. It seems that the phase is distorted by the three slits when |r| > 0.5 mm, but the beam spots are concentrated on the region |r|<0.5 mm from Fig. 6, implying that this disturbance does not play the central role for the EBS in turbulence. From Fig. 7(a-1)–(h-1), one finds that the phase singularity of vortex beams without turbulence exists at the on-axis point, irrespective of the reflector being a flat mirror or a RR. In the presence of turbulence, the phase distribution is severely disturbed by the atmospheric turbulence. Phase singularities may appear in other positions of the beam cross-section for the Gaussian beam or vortex beams, and the on-axis phase singularity of the vortex beams may disappear [see in Fig. 7(b-2), (c-2) and (f-2)]. Since the real atmospheric turbulence are time varying, we can judge that the phase singularity at the on-axis point doesn't exist all the time in turbulence.

Fig. 8 illustrates the average intensity distributions of the Gaussian beam ($l=0$) and vortex beams with $l=1$, 2 and 3 reflected by a flat mirror and a RR. One sees that only when $l=0$, 2 (even number), a bright spot in the beam center appears, indicating the EBS effect. The simulation results agree well with the experimental results shown in Fig. 3. We also plot in Fig. 9 the simulation results of the corresponding instantaneous beam profiles of vortex beams when the mode conversion effect occurs. It is seen that the beam mode converts from the LG_{0l} mode to its corresponding HG_{l0} mode. Our results (not shown here) reveal that the EBS effect only appears for $l=0$, 2 (even number) and the phenomenon of mode conversion also occurs when the introduced three slits in the RR plane is removed in the numerical simulation.

4. Conclusion

In conclusion, we have experimentally measured the average/instantaneous intensity distributions of vortex beams on double-passage in monostatic turbulence using a retroreflector. The experimental results show that EBS occurs only when the topological charge is even, and this can be explained using a model of reciprocal ray pairs. Furthermore, in the instantaneous intensity, the beam may convert from an LG mode to its corresponding HG mode under certain turbulence conditions. This arises because the turbulence acts as an asymmetric cylindrical lens system. Our finds may be useful in FSOC systems using vortex beams and point towards methods for controlling EBS by engineering the phase of the beam.

Acknowledgments

This work is supported by the National Natural Science Fund for Distinguished Young Scholar(11525418); National Natural Science Foundation of China (NSFC) (91750201 & 11474213 & 11874046); Project of the Priority Academic Program Development of Jiangsu Higher Education Institutions; China Scholarship Council (CSC) (201706920103); Qing Lan Project of Jiangsu Province.

Supplementary materials

Supplementary material associated with this article can be found, in the online version, at doi:10.1016/j.jqsrt.2019.02.021.

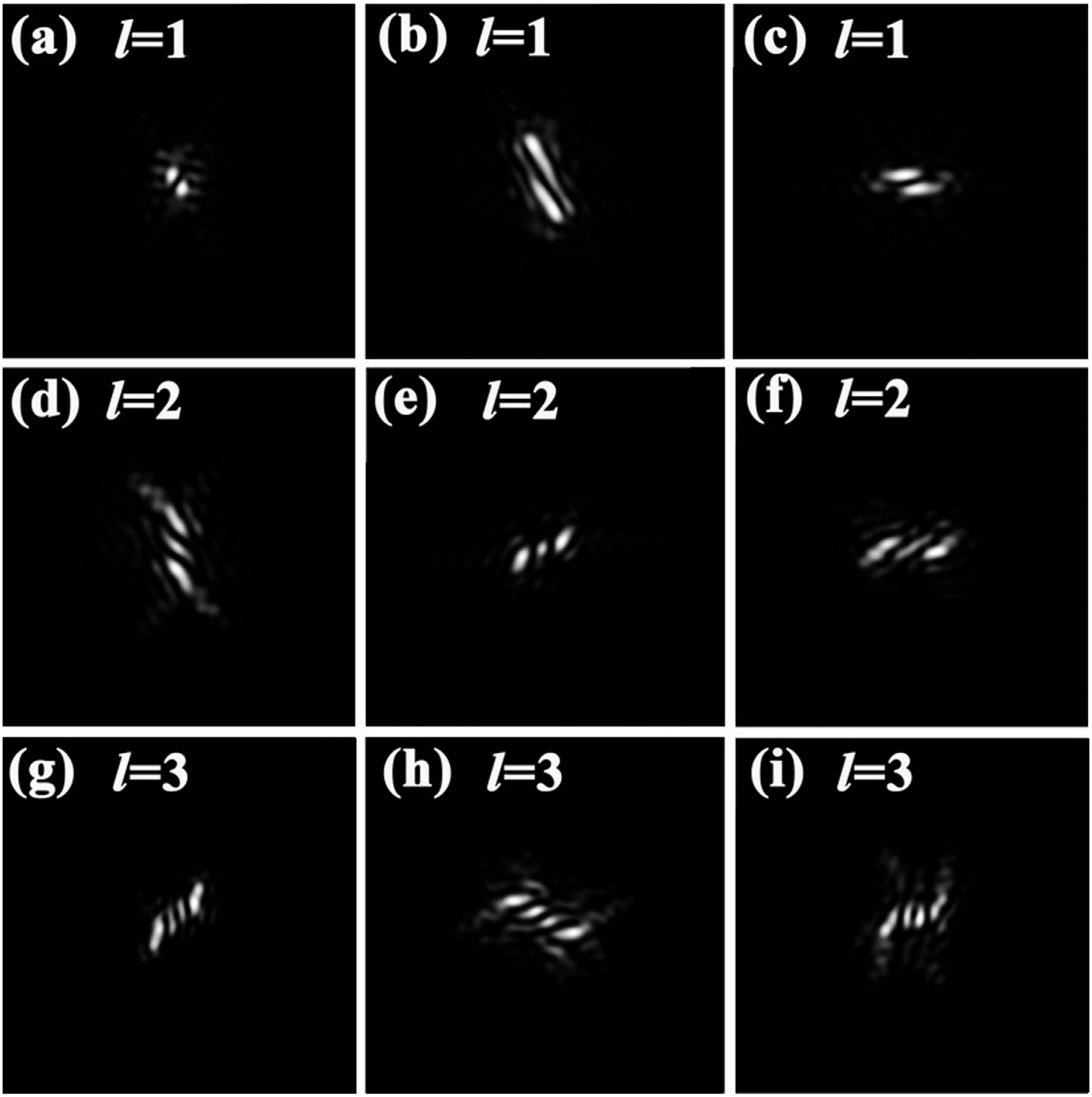

Fig. 9. Simulation results of the instantaneous beam profiles of vortex beams double-passage through the monostatic turbulence with occurrence of the mode conversion. (a)–(c) $l=1$ [media 4], (d)–(f) $l=2$ [media 5], (g)–(i) $l=3$ [media 6]. The size of pictures is 1.5 mm × 1.5 mm.

References

[1] Belen'kii M, Mironov V. Diffraction of optical radiation on a mirror disc in a turbulent atmosphere. Quantum Electron 1972;5:38–45.
[2] Gurvich A, Kashkarov S. Enhanced backscattering in a turbulent medium. Izv Vyssh Uchebn Zaved Radiofiz 1977;20:794–6.
[3] Kashkarov S. Enhancement of the average backscattered intensity in a turbulent atmosphere. Izv Vyssh Uchebn Zaved Radiofiz 1983;26:44–8.
[4] Banakh V, Mironov V. Lidar in a turbulent atmosphere. Artech; 1987.
[5] Barabanenkov Y, Kravtsov Y, Ozrin V, Saichev A. Enhanced backscattering in optics. Prog Opt 1991;29:65–197.
[6] Jakeman E. Enhanced backscattering through a deep random phase screen. J Opt Soc Am A 1988;5:1638–48.
[7] Andrews L, Phillips R, Miller W. Mutual coherence function for a double-passage retroreflected optical wave in atmospheric turbulence. Appl Opt 1997;36:698–708.
[8] Agrovskii B, Bogaturov A, Gurvich A, Kireev S, Myakinin V. Enhanced backscattering from a plane mirror viewed through a turbulent phase screen. J Opt Soc Am A 1991;8:1142–7.
[9] Churnside J, Wilson J. Enhanced backscatter of a reflected beam in atmospheric turbulence. Appl Opt 1993;32(15):2651–5.
[10] Harvey J, Reddy S, Phillips R. Precision pointing and tracking through random media by exploitation of the enhanced back-scatter phenomenon. Appl Opt 1996;35:4220–8.
[11] Smith C, Belichki S, Coffaro J, Panich M, Splitter L, Andrews L, Phillips R, Wayne D. Enhanced backscatter analysis for long-range optical tracking in deep turbulent conditions. Proc SPIE 2015;9614:96140A.
[12] Welch G, Rhodes W. Imaging through a random screen by enhanced backscatter: a physical interpretation. Appl Opt 1993;32:2692–6.
[13] Achour M. Free-space optical communication by retro-modulation: concept, technologies and challenges. Proc SPIE 2004;5614:52.
[14] Amon S, Barry J, Karagiannidis G, Schober R, Uysal M. Advanced wireless optical communication systems. Cambridge University; 2012.
[15] Rabinovich W, Mahon R, Feraro M, Geotz P, Murphy J. Reduction of scintillation in optical modulating retro-reflector links. Opt Express 2014;22:28553–65.
[16] Mahon R, Moore C, Ferraro M, Rabinovich W, Suite M. Atmospheric turbulence effects measured along horizontal-path optical retro-reflector links. Appl Opt 2012;51:6147–58.

[17] Mahon R, Ferraro M, Goetz P, Moore C, Murphy J, Rabinovich W. Irradiance correlations in retro-reflected beams. Appl Opt 2015;54:F96–102.
[18] Yang G, You S, Bi M, Fan B, Lu Y, Zhou X, Li J, Chen H, Wang T. Wave-optics simulation of the double-pass beam propagation in modulating retro-reflector FSO systems using a corner cube reflector. Appl Opt 2017;56:7474–83.
[19] Nelson W, Palastro J, Wu C, Davis C. Enhanced backscatter of optical beams reflected in turbulent air. J Opt Soc Am A 2015;32:1371–8.
[20] Li J, Martinez-Piedra G, Korotkova O. Enhanced Back-Scatter in double-pass optical links with non-classic turbulence. Opt Express 2018;26:10128–39.
[21] Qu J, Zhong Y, Cui Z, Cai Y. Elegant Laguerre–Gaussian beam in turbulent atmosphere. Opt Commun 2010;283:2772–81.
[22] Liu X, Shen Y, Liu L, Wang F, Cai Y. Experimental demonstration of vortex phase-induced reduction in scintillation of a partially coherent beam. Opt Lett 2013;38:5323–6.
[23] Huang Y, Yuan Y, Liu X, Zeng J, Wang F, Yu J, Liu L, Cai Y. Propagation of optical coherence vortex lattices in turbulent atmosphere. Appl Sci 2018;8:2476.
[24] Wang J, Yang J, Fazal I, Ahmed N, Yan Y, Huang H, Ren Y, Yue Y, Dolinar S, Tur M, Willner A. Terabit free-space data transmission employing orbital angular momentum multiplexing. Nat Photon 2012;6:488.
[25] Gbur G, Tyson R. Vortex beam propagation through atmospheric turbulence and topological chargeconservation. J Opt Soc Am A 2008;25:225–30.
[26] Lavery M, Peuntinger C, Gunthner K, Banzer P, Elser D, Boyd R, Padgett M, Marquardt C, Leuchs G. Free-space propagation of high-dimensional structured optical fields in an urban environment. Sci Adv 2017;3:e1700552.
[27] Rodenburg B, Lavery M, Malik M, O'Sullivan M, Mirhosseini M, Robertson D, Padgett M, Boyd R. Influence of atmospheric turbulence on states of light carrying orbital angular momentum. Opt Lett 2012;37:3735–7.
[28] Malik M, Lavery M, Malik M, O'Sullivan M, Mirhosseini M, Robertson D, Padgett M, Boyd R. Influence of atmospheric turbulence on optical communications using orbital angular momentum for encoding. Opt Express 2012;20:13195–200.
[29] Paterson C. Atmospheric turbulence and orbital angular momentum of single photons for optical communication. Phys Rev Lett 2005;94:153901.
[30] Vaziri A, Pan J, Jennewein T, Weihs G, Zeilinger A. Concentration of higher dimensional entanglement: qutrits of photon orbital angular momentum. Phys Rev Lett 2003;91:227902.
[31] Yuan Y, Liu D, Zhou Z, Xu H, Qu J, Cai Y. Optimization of the probability of orbital angular momentum for Laguerre–Gaussian beam in Kolmogorov and non-Kolmogorov turbulence. Opt Express 2018;26:21861–71.
[32] Tamburini F, Anzolin G, Umbriaco G, Bianchini A, Barbieri C. Overcoming the Rayleigh criterion limit with optical vortices. Phys Rev Lett 2006;97:163903.
[33] Krenn M, Fickler R, Fink M, Handsteiner J. Communication with spatially modulated light through turbulent air across Vienna. New J Phys 2014;16:113028.
[34] Heckenberg N, McDuff R, Smith C, White A. Generation of optical phase singularities by computer-generated holograms. Opt Lett 1992;17:221–3.
[35] Courtial J, Padgett M. Performance of a cylindrical lens mode converter for producing Laguerre–Gaussian laser modes. Opt Commun 1999;159:13–18.
[36] Andrews L, Phillips R. Laser beam propagation in turbulent atmosphere. SPIE press; 2005.
[37] Schmidt J. Numerical simulation of optical wave propagation with examples in MATLAB. SPIE; 2010.
[38] Gbur G. Partially coherent beam propagation in atmospheric turbulence [Invited]. J Opt Soc Am A 2014;31:2038–45.
[39] Wang F, Liu X, Cai Y. Propagation of partially coherent beam in turbulent atmosphere: a review [Invited Review]. PIERS 2015;150:123–43.
[40] Wang F, Yu J, Liu X, Cai Y. Research progress in propagation of partially coherent beams in turbulent atmosphere. Acta Phys Sin 2018;67:184203.